IEEE Access
Multidisciplinary ⋮ Rapid Review ⋮ Open Access Journal

Received 13 January 2023, accepted 13 February 2023, date of publication 6 March 2023, date of current version 13 March 2023.

Digital Object Identifier 10.1109/ACCESS.2023.3252891

RESEARCH ARTICLE

An Innovative Converterless Solar PV Control Strategy for a Grid Connected Hybrid PV/Wind/Fuel-Cell System Coupled With Battery Energy Storage

MUHAMMAD MAJID GULZAR[1,5], AYESHA IQBAL[2], DAUD SIBTAIN[3], AND MUHAMMAD KHALID[4,5,6], (Senior Member, IEEE)

[1]Control and Instrumentation Engineering Department, King Fahd University of Petroleum and Minerals (KFUPM), Dhahran 31261, Saudi Arabia
[2]Department of Electrical Engineering, University of Central Punjab, Lahore 54000, Pakistan
[3]Energy Center of Excellence (ECoE), Harbin Electric International, Harbin 150028, China
[4]Electrical Engineering Department, King Fahd University of Petroleum and Minerals (KFUPM), Dhahran 31261, Saudi Arabia
[5]Center for Renewable Energy and Power Systems, King Fahd University of Petroleum and Minerals (KFUPM), Dhahran 31261, Saudi Arabia
[6]SDAIA–KFUPM Joint Research Center for Artificial Intelligence, King Fahd University of Petroleum and Minerals (KFUPM), Dhahran 31261, Saudi Arabia

Corresponding author: Muhammad Khalid (mkhalid@kfupm.edu.sa)

This work was supported by the Center of Renewable Energy and Power Systems, King Fahd University of Petroleum and Minerals (KFUPM) under Project INRE2220. The work of Muhammad Khalid was supported by the SDAIA–KFUPM Joint Research Center for Artificial Intelligence (JRC-AI).

ABSTRACT The proposed work addresses the modeling, control, energy management and operation of hybrid grid connected system with wind-PV-Battery Energy Storage System (BESS) integrated with Fuel Cell (FC) and Electrolyzer. A hybrid PV-Wind-FC with electrolyzer consisting of BESS with the least number of control loops and converters has been proposed. The proposed hybrid system presents a cost efficient solution for integrating PV into a hybrid system by eliminating the PV converter. This includes the design of controllers for grid-connected hybrid systems with a renewable distributed generator (Wind and PV) as a primary source, BESS as a secondary source and FC with Electrolyzer as a tertiary source. In addition, the lead compensator along with integrator is used for obtaining enough phase margin and removing steady state error completely. It increases the stability of the controller and adds phase shift φ_s at a cross gain frequency (ω_{cut}). The Grid Side Controller (GSC) is capable of providing frequency support to the utility grid, when it is linked to the grid. In the proposed configuration, PV power is maximized and injected into grid through GSC. Rotor Side Converter (RSC) and GSC ensure the support for sharing the burden of the grid station. Moreover, the proposed controller of BESS with coordination of FC eliminates the effect of intermittency of power generated from wind and PV. Excess power production by renewable distribution generation is used by Electrolyzer to generate hydrogen. This hydrogen is further used by FC when there is not enough power generation due to unfavorable weather conditions. The energy management has been presented to fulfill the load profile, avoid BESS overcharging and to minimize the intermittency and fluctuation of Wind and PV sources. This method guarantees steady power flow and service continuity. The Simulink model of the proposed system results validate the efficiency of the proposed hybrid system as compared to the conventional hybrid system reported in the literature. The modeling of the proposed system and analysis has been demonstrated using the MATLAB Simulink model. Lastly, the energy management of the system has also been examined and compared with the conventional power system.

INDEX TERMS Grid-connected system, energy management system, battery energy storage system, electrolyzer, fuel cell, doubly fed induction motor, maximum power point tracking.

The associate editor coordinating the review of this manuscript and approving it for publication was Mouloud Denai.

I. INTRODUCTION

An increase in number of home appliances to do simple tasks of the household has made life very relaxed and effortless. Whereas with the inclusion of each electric appliance at home the electric demand is growing. Power generation is continuously increasing to fulfill the electric power demand. Renewable and non-renewable generations are added to the power network to meet the demand. All different types of conventional and non-conventional sources bring different types of complexities to the power flow architecture. With growing environmental concerns during the last few decades, governments are putting effort to include renewable generation into the national grid to meet the total electric demand. The renewable energy sources which are PV, FC, ultra-capacitor, WT, geothermal, etc., are integrated into the existing power generation architecture for clean and green energy [1], [2]. Most frequent used renewable generation sources are solar cells and wind turbines due to their easy installation and cost-to-power ratio and these two sources are adopted in different typologies throughout the world as no fuel is required for the power generation [3], [4], [5] (unlike fuel cell stack, biogas etc.).

Wind turbines are coming out to be very reliable power generation sources due to their power regulation characteristics. With the development of new types of wind turbine generation architecture, off-shore topology wind turbines are a hot topic of research these days. Speed regulation control of wind turbine in a Doubly Fed Induction Generators (DFIGs) a very efficient power generation source. Maximum power point tracking (MPPT) of the power which is generated by the turbine can be accomplished by controlling the speed of the rotor based on wind speed [6]. In the recent few decades, multiple control architectures have been proposed by researchers to improve the efficiency of the DFIG power generation turbines [7], [8], [9], [10], [11]. Liu et al. [10] and Xu et al. [11] have presented some advanced control algorithms to decrease transient oscillations delivered to the stator from the rotor side due to wind speed variations. A voltage conditioning architecture has been proposed by Nian and Song [12] which decreases the harmonics in the current and voltage by performing smooth transitions and overall smoothing the active and reactive power generation in a DFIG power generation architecture. Contrary to wind power generation PV array is a very efficient and easy-to-handle power generation. There is no noise pollution, air pollution or mechanical maintenance as compared to wind turbines. Very large PV farms have been introduced with several gigawatt power generation capacity making them reliable power generation to meet the growing demand of the electric power [13], [14]. Electric power from the PV array is integrated into the grid by using two basic topologies: single stage or two-stage. The single stage has less number of converters and power switches but the control architecture to make the operation possible has its complexity compared to the two-stage integration topologies. Voltage Source Inverter (VSI) topology is generally used to control the injecting power to the grid.

Power generation using hybrid topology has gained a lot of attention due to its economical and Eco-friendly benefits. The power grids attached to PV and wind turbines show more stability due to the complementary power generation and can be installed in divergent weather conditions [15], [16], [17], [18]. It is being observed that the above two types of sustainable sources have another option and development [19], [20], [21]. Generally, at day time, the production of power from PV is more and the production of power from the wind turbine is less. But at night time, the production of PV is insignificant and nearly zero, because of more speed of wind in contrast to the day time, the power produced from the turbines of wind increases decisively. The corresponding element is likewise observed in various seasons. Like during summer season, when there is more power from the sun, wind is less accessible, while during winter season, the velocity of the wind is higher and the viable energy from the sun is less. Such element has persuaded various analysts to look for approaches to combine two energy sources. This assimilation prompts a couple of issues concerning the quality of the power, validity, and steadiness of the whole system [22]. The feasible solution which exhibits low fluctuation of power, enhanced quality of the power, energy and less unbalance because of the renewable sources which are given by Electrical Energy Storage Systems (EESSs) [23], [24], [25]. Reasonable EESSs could have given a critical way to deal with the unreliability and irregularity of the Renewable Energy Sources (RES) generations [26], [27], [28]. In general, EESS enables reliable generation of power that can be used when the costs of generation are high, demand is high, or other means of generation of power are not available [23], [29], [30]. Several energy storage systems are divided on the basis of the two criterion: form and function. On the basis of functional criteria, EESS are divided into high ratings of power, which includes supercapacitors, Super-Conducting Magnetic Energy Storage (SMES), batteries and flywheels [30], and for the management of energy, such as FCs, bulk batteries, Solar cells, and the flow batteries [31], [32], [33]. On the basis of form, electrical energy is being stored in multiple ways, e.g., as storage of chemical energy, as storage of thermal energy, as storage of mechanical energy, and it can be transformed into power whenever required. EESS is the preferred option to endure variations of power and assures sovereignty in hybrid grid systems. Therefore, the Hybrid Energy Storage System (HESS) is a need of the hour [34], [35], [36]. So, the charging cycles and the discharging cycle of the battery have a significant impact on the service life of these systems [37], [38], [39]. A source of third energy is therefore absolutely necessary for the improvement of the security of the supply of energy of PV and Wind turbine system. A third power system should be selected according to the benefits and form of the storage system.

Various studies on this area has shown the chance of increasing PV systems with wind turbines with minimal adjustments. To consolidate the wind turbine and the PV in a hybrid system, [4] have utilized a converter of a three-phase square waveform. To work more on the DC loads of hybrid system, another three-input dc-dc boost converter is being presented in [40]. Whereas, in hybrid system the expansion of the above converters is not reasonable. An arrangement of Wind & PV power concentrating on the smooth variation of the DC voltage and the reduced size of the DC capacitor bank has been established in [41]. In [42] and [43], the state of charge (SOC) of the BESS has been controlled in the systems to decrease the variation of the output power. References [44] and [45] have presented new approaches for examining and improving the structures by utilizing battery energy systems.

Many researches have been produced to propose novel control strategies for the hybrid system. By focusing on fifth and seventh grid voltage harmonics, [12] proposed a modified control algorithm for smoothing hybrid system active and reactive output power. A control scheme of two-layer constant power for wind farms equipped with DFIGs has been reported in [46]. In this work, Super-Capacitor (SC) as an energy storage system and DFIG DC link is linked with each other. New cost minimization and power generation has been presented in [47] for hybrid RES. The control structure for the battery bank has just a control loop presented in this work. The study in [48], proposed an embedded energy share method between battery and SC which are designed to meet peak power requirements whereas battery fulfills average power. In the first topology, battery is being attached to the DC bus through the DC-DC buck-boost converter and converter has been removed in the second configuration. DC-DC converter has also been used between DC bus and SC for power exchange. The research in [49], describes a method for providing voltage and frequency support to an islanded microgrid by coordinating and integrating the operation of solar generators (PV) with control of MPPT and battery storage. The control loop method is used in this work for controlling the battery energy storage system. In addition, PV//MPPT/battery with active power control and the reactive power control has been implemented for grid tied (hybrid) systems. The control algorithms demonstrate efficient correspondent of the control of inverter, discharging and the charging of the energy storage and MPPT.

So, the mentioned studies did not consider the efficiency and optimality of the proposed structure and only focused on the control design and power energy sources coordination. Also, no optimization has been done considered for hybrid energy system efficiency.

The promising architecture of a system with DFIG and PV has been proposed by [19] in which the PV converter has been omitted. It should be noted that PV capacity and PV converter rating should be the same. In this research, the authors demonstrated that PV capacity may be significantly greater than the grid side controller (GSC) rating. The utilization of the new converter increases after consolidating the converter of PV and GSC. Implementation of MPPT in [19] can be done by controlling DC link voltage. However, this configuration observed large power output fluctuation and under normal conditions, large oscillations occurred in DC link voltage. Due to the intermittent nature of PV and wind, if wind speed and solar irradiation are low or high, the requirement of power of the system can be curtailed. However, this design is incapable of extracting maximum solar energy. Also, GSC is not used to its full potential.

To meet the shortcoming of [19] and [50] introduced BESS to the PV-DFIG hybrid system with a reduced control scheme. The oscillations in DC link voltage and GSC power have been stabilized up to a large extent. In this proposed configuration utilization of GSC has been improved and DC bus capacitor size has decreased. However, charging of the Battery and the discharging of BESS decreases the life span of batteries. Moreover, BESS alone cannot cater to the load demand when Wind and PV supply less power to DC links due to weather conditions. In this process, persistant charging of battery and the discharging decrease the lifespan of the BESS. Therefore, another energy source is needed to back up the supply to the grid-connected system and load.

In this paper, FC and Electrolyzer as a third energy source has been added to the PV-DFIG and BESS hybrid grid connected system. A hybrid PV-Wind-BESS with FC and electrolyzer with the least number of control loops and converters have been proposed. The proposed hybrid system presents a cost efficient solution for integrating PV into a hybrid system by eliminating the PV converter. This includes the design of controllers for grid-connected hybrid systems with a renewable distributed generator (Wind and PV) as a primary source, BESS as a secondary source and FC with Electrolyzer as a tertiary source. The main research objectives and advantages of the proposed system are:

- To establish an efficient and cost-effective setup of PV-DFIG-BESS with reduced control loops with FC and Electrolyzer.
- To perform common AC and DC bus voltage and MPPT by the controller of GSC.
- To minimize GSC power and DC link voltage fluctuation to large extent.
- New topology for hybrid Wind, PV, BESS, FC with Electrolyzer to achieve optimal and efficient control of the different sources, ensuring better power quality for AC grid, regulating the voltage level and the frequency of AC grid, ensuring continuity of the service.
- Implementation and integration of FC and Electrolyzer to make the system more sustainable when Wind and solar PV power depend on weather conditions and during night hours solar power is zero. Therefore, under the situation of long-term, no-wind and solar PV or low-wind and solar conditions, BESS alone cannot cater to the load demand.
- To provide frequency support to the AC side while ensuring stable operation of the DC side.

- To demonstrate the effectiveness of the proposed setup on MATLAB Simulink.

The rest of the paper is organized as: A description of the proposed hybrid grid-connected system is explained in section II. Section III demonstrates system modeling and control. In Section IV, energy management is given. Section V demonstrates the system simulation and results. The conclusion is presented in Section VI.

II. DESCRIPTION OF PROPOSED HYBRID GRID CONNECTED SYSTEM

The configuration of the proposed system is shown in Fig. 1. The GSC and its control scheme used in the proposed system are meant to limit the DC-bus voltage and to maintain it within its prescribed safe limits.The voltage of the DC-link also makes the system enable to track MPP for the PV system. To protect the GSC against overloads, a BESS is coupled with the system. The BESS is used as a storage device and is connected to the DC bus through DC/DC Buck-Boost bidirectional converter. As PV and wind power depend upon weather conditions while PV power is zero at night time. Thus, the battery alone cannot cater to the full load demand when there is zero wind and PV energy or less wind. Therefore, in order to make the system more sustainable, FC with an electrolyzer is integrated with the system. When there is high-power generation from PV and wind sources, the battery reached its threshold limit of charge storage, then the electrolyzer activates and stores surplus energy. The electrolyzer generates hydrogen that can be stored and used by FC as input. FC use hydrogen to generate power when there is not enough power generation at the DC link due to unfavorable weather conditions.

III. SYSTEM MODELLING AND CONTROL

A. MODEL DEVELOPMENT FOR SOLAR PV

There are a number of solar cells inside a PV array and these cells generate charge carriers whenever photons fall on the array. The electrons are ejected out and make the current flow if the energy of the photon is more than the band gap of the semiconductor. Various poly-crystalline solar cells are cost-effective and easily affordable along with the typical mono-crystalline solar cells. In order to find out a correct solar equation that may correlate to real-world behavior, a lot of research has been done so far. So, the characteristics of cells of the PV arrays are not satisfactory. The ideal model of the PV array is a diode in parallel connection and a current source. In Fig. 2, the single solar cell circuit is being presented that is comprised of a current source and Shockley diode with parallel resistance R_{per} and series resistance R_{ser}. The combination of diode current and current source is summed up as the total current of the solar cell [51].

The mathematical expression for single solar cell is illustrated in eq. (1).

$$I = I_{PV} - I_o\left[e^{\frac{qV}{akT}} - 1\right] \tag{1}$$

where, I is single solar cell current, I_{PV} is solar irradiation total generated current, I_o is reverse leakage current (saturation), a is Diode factor, T is Diode temperature (Kelvin), q is electron charge and k represent Boltzmann constant.

All features of the solar cell are not presented in eq. (1). Inculcation of both series and parallel resistances makes this model as the best one particular for empirical conditions. R_{ser} is termed as the resistance between the solar cell and terminal connection.

$$I = I_{PV} - I_o\left[e^{\frac{V+R_{ser}I}{V_t a}} - 1\right] - \left(\frac{V + R_{ser}I}{R_{per}}\right) \tag{2}$$

where R_{ser} is total series resistance, R_{per} is total parallel resistance, V_t is thermal voltage and can be further calculated using expression, $V_t = kT/q$; where V is combined terminal voltage of the solar cells. R_{per} is resistance produced from p-n junction leakage current.

On the basis of parallel and series configurations of PV array's solar cells, the eq.(2) can be changed. If the number of parallel cells is increased, the current level of a PV array is also increased. Similarly, when the number of series cells is increased, the voltage of a PV array is also increased.

Charges produced because of temperature and solar irradiation is I_{pv} as depicted in eq. (3).

$$I_{pv} = \left(I_{pvn} - K_i\Delta T\right)\frac{G}{G_n} \tag{3}$$

As parallel resistance of the solar cell is greater than series resistance thus, the short current is approximately equal to PV threshold current. I_{pvn} is threshold PV current, K_i is Current coefficient, T is Difference between nominal and actual temperature $K: T_n - T$, G is incident solar radiation and G_n is nominal solar radiation. Units of G_n and G are W/m^2. A lot of work has been done in this domain and many formulas for features of solar cells and their designs are developed. Here the I_{on} is given as eq. (4).

$$I_{on} = \frac{I_{sen} + K_i\Delta T}{e^{\left(\frac{V_{ocn}+K_v\Delta T}{a V_t}\right)-1}} \tag{4}$$

where, V_{ocn} is Open circuit nominal voltage, K_v is Voltage coefficient, I_{scn} represents Nominal short-circuit current, a is Ideal diode factor, V_t is the thermal voltage. For modeling solar cells, eqs. (1), (2) and (3) are used together. Temperature and irradiation are the factors that have a direct relation to the operation of the solar cell.

B. MODEL DEVELOPMENT FOR WIND TURBINE

The aerodynamic power of the wind turbine is illustrated in eq. (5)

$$P_m = \frac{1}{2}\rho\, C_p\,(\beta, \lambda)\, A\, v_t^3 \tag{5}$$

where, P_m represents mechanical power taken by the wind turbine, V_t is the wind speed, C_P shows the power coefficient, λ is the speed ratio, β represents blade angle and A is area rotor blades.

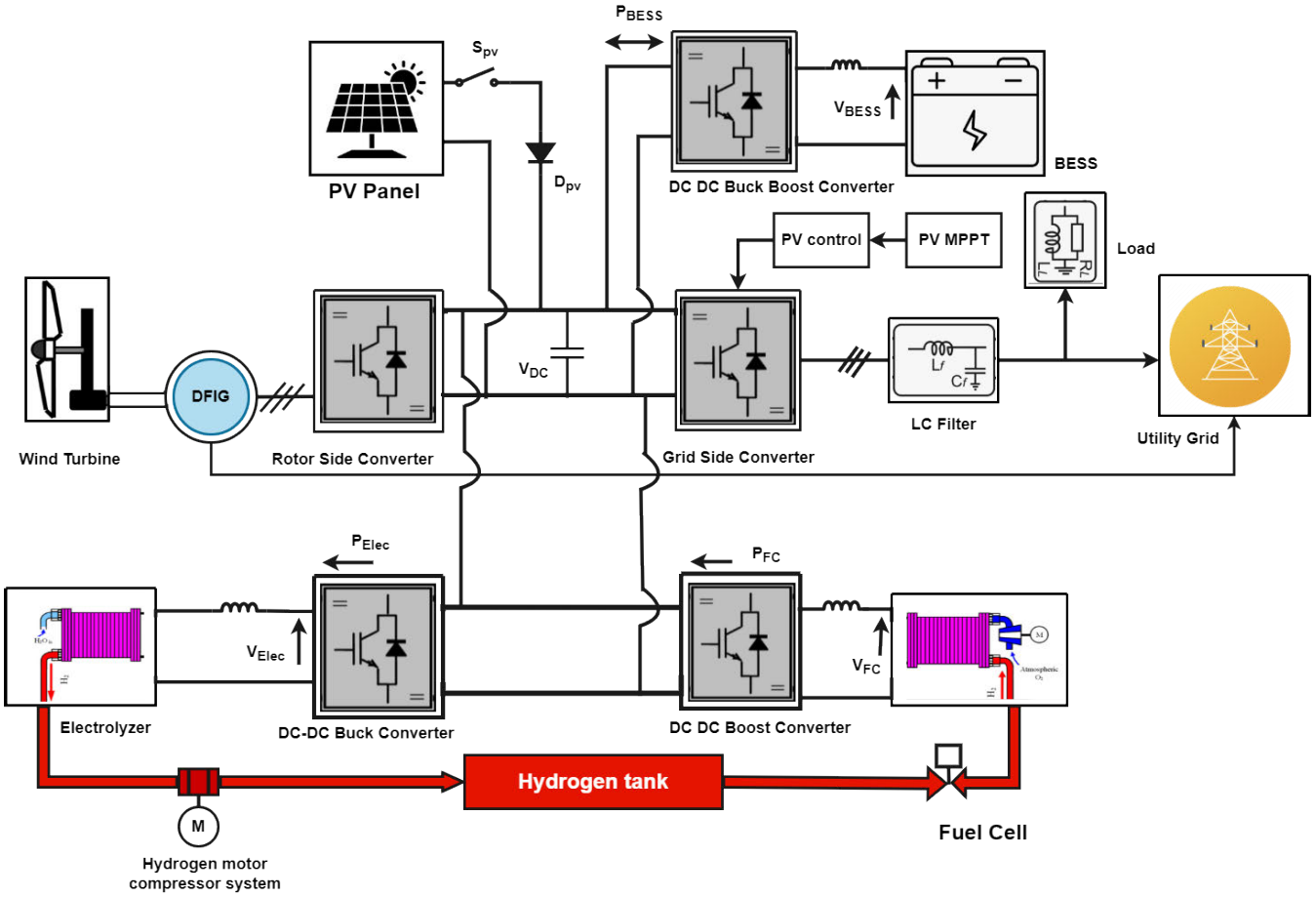

FIGURE 1. Structure of proposed grid connected hybrid system.

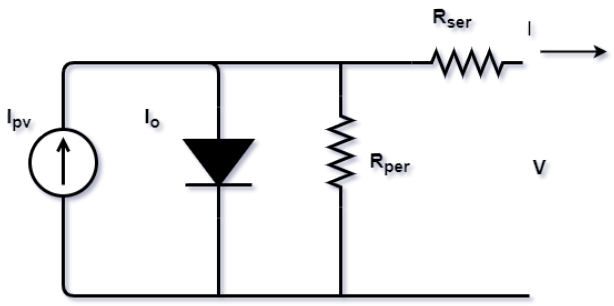

FIGURE 2. Equivalent circuit of single solar cell.

In the proposed hybrid system, a model based on voltage-flux equations in the d-q reference frame is used to regulate the DFIG [52]. In this model, d-axis of the frame has an alignment with the flux space vector of the stator that further rotates with synchronous speed. About the components of the rotor current, the equation of rotor and stator can be represented as eq. (6).

$$\begin{aligned} \sigma L_r \frac{di_{dr}}{dt} &= -R_r i_{dr} + \omega\sigma L_r i_{qr} + v_{dr} - \frac{L_m}{L_s}\frac{d}{dt}\varphi_{ds} \\ \sigma L_r \frac{di_{qr}}{dt} &= -R_r i_{qr} + \omega\sigma L_r i_{dr} + v_{qr} - \frac{L_m}{L_s}\frac{d}{dt}\varphi_{qs} \end{aligned} \tag{6}$$

Here, rotor current and terminal voltage components are v_{qr}, v_{dr}, i_{qr} and i_{dr} respectively. ω_r and ω_o are rotor and synchronous speeds (rad/sec). Where as: $\omega = \omega_o - \omega_r$. The components of star flux in d-q reference are taken as φ_{qs} and φ_{ds}. R_r used here represents resistance of rotor winding. σ is the leakage component and it can be written mathematically as eq. (7).

$$\sigma = \frac{L_r L_s - L_m^2}{L_s L_r} \tag{7}$$

Here L_r, L_m and L_s represent various inductance. T_e represents electromagnetic torque of machine given as eq. (8).

$$T_e = -p\frac{3L_m v_{ms}}{2L_s\omega_o} i_{qr} \tag{8}$$

where, v_{ms} represents the amplitude of stator voltage. P_e denotes electromagnetic power that can be expressed mathematically as eq. (9).

$$P_e = -\frac{3L_m\omega_r}{2L_s\omega_o} v_{ms} i_{qr} \tag{9}$$

Likewise, using eq.(9), rotor power (P_r) and stator power (P_s) equations are given as eq. (10).

$$P_r = -\frac{3L_m}{2L_s} v_{ms} i_{qr}$$
$$P_s = -\frac{3L_m\,(\omega_o - \omega_r)}{2L_s\omega_o} \frac{L_m}{L_s} v_{ms} i_{qr} \tag{10}$$

1) RSC CONTROL

The components of terminal voltage v_{qr} and v_{dr} are controlled by the RSC. A sinusoidal pulse along with modulation indices m_{qr} and m_{dr} are used here to control voltage components. The product of i_{qr} and i_{dr} variables make the rotor current model non-linear. To find out rotor terminal voltage, the rotor current dynamics are separated by using the expression:

$$\sigma L_r \frac{di_{dr}}{dt} = -R_r i_{dr} + g_1$$
$$\sigma L_r \frac{di_{qr}}{dt} = -R_r i_{qr} + g_2 \tag{11}$$

Here, g_1 and g_2 are the two new parameters of control that depends upon m_{qr} and m_{dr}, given as:

$$m_{dr} = \frac{2}{V_{DC}} \left(g_1 - \omega\sigma L_r i_{qr}\right)$$
$$m_{qr} = \frac{2}{V_{DC}} \left(g_2 - \omega\sigma L_r i_{qr} + \frac{L_m\omega}{L_s\omega_o} v_{ms}\right) \tag{12}$$

where, V_{DC} represents DC-link voltage. Transfer function for i_{qr} and i_{dr} currents can be obtained using eq.(12), such as:

$$G_{ir}(s) = \frac{I_{dr}(s)}{G_1(s)} = \frac{I_{qr}(s)}{G_2(s)} = \frac{1}{\sigma L_r s + R_r} \tag{13}$$

In order to control components of rotor current, Proportional Integral (PI) controller is composed which is implemented on the fundament of the zero pole cancellation method. The zero of the plant transfer function is expressed as $S_Z = -\frac{K_{Ir}}{K_{Pr}}$, and its pole is given as $S_P = -\frac{R_r}{\sigma L_r}$. While K_{Ir} represents integral gain and K_{pr} denotes proportional gain of PI controller. The value of the closed-loop current control time constant T_{cr} is kept quite small to achieve appropriate bandwidth, and it is kept at 1/10th of the switching frequency. On the basis of these criteria, the factors of the PI controller are expressed as:

$$K_{pr} = -\frac{\sigma L_r}{T_{cr}}, \quad K_{Ir} = -\frac{R_r}{T_{cr}} \tag{14}$$

The active power and the reactive power of the circuit of the stator [52] are expressed as:

$$Q_s = \frac{3v_{ms}^2 L_m}{2\omega_o L_s} - \frac{3}{2}\frac{v_{ms}^2 L_m}{L_s} i_{dr}$$
$$P_s = -\frac{3L_m}{2L_s} v_{ms} i_{dr} \tag{15}$$

In order to avoid high rotor currents and RSC loading, the set point for i_{dr} is generally taken as zero. Thus, the block diagram of RSC control is shown in Fig. 3

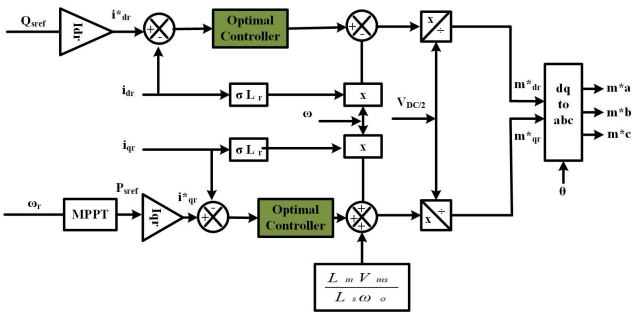

FIGURE 3. Control Scheme of RSC.

2) GSC CONTROL

The GSC control is meant to control DC-link voltage in the proposed model. MPPT for PV is also maintained and tracked using P&O algorithm. Initially, components of the current of GSC are being decoupled as:

$$L_g \frac{di_{dg}}{dt} = -R_g i_{dg} + L_g\omega_o i_{qg} - v_{dg} + \frac{v_{DC}}{2} m_{dg}$$
$$L_q \frac{di_{dq}}{dt} = -R_q i_{dq} + L_g\omega_o i_{dg} - v_{qg} + \frac{v_{DC}}{2} m_{qg} \tag{16}$$

where V_{qg} and V_{dg} are components of grid voltage. In this scanrio, the stator voltage vector has been aligned in d-axis of the reference frame thus, $V_{qs} = 0$. When new variables such as J_{dq} and J_{dg} are inaugurated, thus the transfer function for the proposed system is obtained as:

$$G_{ig}(s) = \frac{I_{dg}(S)}{J_{dg}(S)} = \frac{I_{qg}(s)}{J_{dq}(s)} = \frac{1}{L_g s + R_g} \tag{17}$$

Modulation indices m_{qg} and m_{dg} are expressed as:

$$m_{dg} = \frac{2}{V_{DC}} \left(J_{dg} - \omega_o L_g i_{qg} + V_{dg}\right)$$
$$m_{qg} = \frac{2}{V_{DC}} \left(J_{qg} + \omega_o L_g i_{dg}\right) \tag{18}$$

To determine the parameters of the current controller G_{cig}, a similar strategy is used. While, K_{Iig} is the integral gain and K_{pig} is the proportional gain, illustrated below as:

$$K_{pig} = \frac{L_g}{T_{cig}}, \quad K_{\text{lig}} = \frac{R_g}{T_{cig}} \tag{19}$$

Closed loop transfer function G_{CL} is used for reducing first-order function, such as:

$$G_{CL} = \frac{1}{T_{cig}S + 1} \tag{20}$$

The balance of electrical Power between the dc side and the ac sides of the GSC is maintained by designing a loop of voltage control that couples the DC-link with the PV and can be expressed as.

$$P_{PV} = \frac{d}{dt}\frac{1}{2} C_{DC} V_{DC}^2 + P_r + \frac{3}{2} V_{dg} i_{dg} + P_{BESS} \tag{21}$$

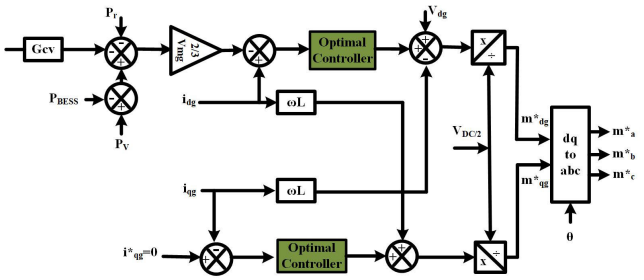

FIGURE 4. Control scheme of GSC.

$i*_{dq}$ is used as control variable instead of i_{dq} when T_{cig} value is kept very small. Moreover, the transfer function using new variable P_c will become:

$$G_v(S) = \frac{{V_{DC}}^2}{P_c} = \frac{2}{C_{DC}S} \tag{22}$$

When, $i*_{dq}$ is quite relevant to P_c, thus it can be expressed as:

$$i*_{dg} = \frac{2}{3V_{dg}}\left(-P_c + P_{pV} - P_r + P_{BESS}\right) \tag{23}$$

PI controller is not compatible to contain nonlinearities produced due to G_v (S) nature. Lead compensator along with integrator is used for obtaining enough phase margin and removing steady state error completely. It increases the stability of the controller and adds phase shift φ_s at a cross gain frequency (ω_{cut}). Transfer function of controller at ($\omega_{cut} = 0.2\frac{1}{T_{cig}}$) is expressed mathematically as:

$$G_{cv}(S) = \frac{K_{lvg}}{s}\frac{s + \frac{r}{\alpha}}{s + r} \tag{24}$$

Here, α and r are lead compensator parameters. Thus, the block diagram of GSC control is shown in Fig. 4

C. MODEL DEVELOPMENT OF BESS

The standard BESS model is selected and modeled as: [53], [54]:

$$\mathrm{V_{Bat}} = \mathrm{E} - \mathrm{R_b} \cdot \mathrm{I_{Bat}} \tag{25}$$

$$E = E_0 - K \cdot \frac{Q}{Q - k \cdot \int i_1 dt} + A \cdot \exp\left(-B \cdot \int i_1 dt\right) \tag{26}$$

$$\mathrm{SOC}(\%) = 100\left(1 - \frac{Q_\mathrm{d}}{\mathrm{C_{bat}}}\right) = 100\left(1 - \frac{\mathrm{I_{bat}}}{\mathrm{C_{bat}}}\mathrm{t}\right) \tag{27}$$

where V_{Bat}, I_{Bat}, Q_d, and C_{Batt} are BESS voltage, current, stored current hour and internal capacity respectively. The BESS SoC and electricity stored during charge are the important parameters that need to be controlled. The supervisory control system must detect BESS SoC and take decisions according to its status and required power.

D. MODEL DEVELOPMENT OF FC

Nowadays, renewable energy sources have attracted the attention of the masses because they are considered an inescapable solution to reduce pollution as well as the dependence of society on fossil fuels. As renewable energy sources produce hydrogen, therefore, its utilization as an energy carrier is thought of as an exhilarating choice in transition of energy trends. The Solid Oxide Fuel Cell (SOFC) is an effective cell among all types of fuel cells because it is 70% efficient. The main two tenets of SOFC over low-temperature types make it more attractive. First, SOFC cells operate at usually high temperatures that permit direct inner handling of fuel in them such as natural gas. Second, these cells get more electric efficiencies easily and this thing makes them reliable for fuel-effective stationary power generation. Therefore, such characteristics reduce intricacy of the system as compared to power plants of low temperature which need hydrogen production with an extra process unit. As fuel cells having high-temperature cannot be turned off easily, therefore, they are acceptable in the stationary sector only. This is the reason that SOFC cells are mostly used in the commercial system which has more working life. Furthermore, excess water can also be transferred again through the steam turbines to generate more electrical power that enhances effectiveness of the system. The SOFC is comprised of two electrodes that are segregated with an electrolyte. The cathode terminal is fed with oxygen while the anode terminal is fed with hydrogen [55]. Thus, reduction takes place at the cathode while oxidation takes place at the anode. The electrolyte permits the passage of ions and electrons that are lost due to oxidation and they move from anode to cathode through an external circuit. This rule is common for all the FC. The kind of geometry, electrolyte and supply of gas vary from one type to another, as presented in Fig. 5.

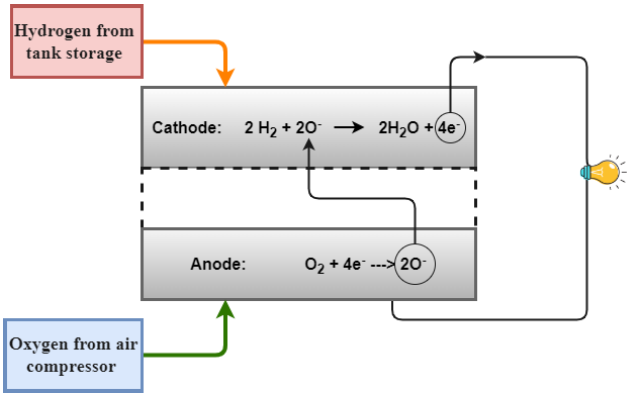

FIGURE 5. Schematic diagram of the Fuel Cell (SOFC type).

The fuel cell is a reliable and auspicious technology for direct power generation and micro-grid applications. Moreover, it is such a component that converts chemical energy to electrical energy with higher efficiency [53].

The ideal voltage of open circuit cell can be determined by the Nernst expression as:

$$V_{Nernst} = -\frac{\Delta G}{2F} - \frac{RT}{2F} ln\left(\frac{P_{H_2O}\, P_{ref}^{0.5}}{P_{H_2}\, P_{O_2}^{0.5}}\right) \tag{28}$$

where, V_{Nernst} denotes Nernst voltage defined as the thermodynamic potential of the cell known as reversible voltage, P_{ref} represents standard pressure (0.1 MPa), and ΔG denotes Gibbs free energy from the reaction. When the electrical cell circuit is being closed, the Nernst potential is reduced and it is given as:

$$V_{cell} = V_{Nernat} - A_{cell}\, ln(\frac{i_{cell}}{i_o}) - i_{cell} R_{incell} - B_{cell}\, ln\,(1 - \frac{i_{cell}}{i_L}) \quad (29)$$

where, V_{cell} denotes cell voltage in the stack. R_{incell} represents inherent fuel cell resistance. Moreover, i_{cell}, i_L and i_o denote the exchange current (Operating) of the cell and the current that is restricted on which fuel is consumed at a rate equivalent to its greatest supply rate, respectively. A_{cell} and B_{cell} denote the numerical coefficients. The ideal gas equations are used to determine the instantaneous change in partial pressures of water vapor and hydrogen in an anode gas flow channel, such as [56]:

$$\frac{dp^{ch}_{H_2}}{dt} = \frac{RT}{V_a}\left[\frac{2M_a}{P^{ch}_a}\left(P^{in}_{H_2} - p^{ch}_{H_2}\right) - \frac{i}{2F}\right] \quad (30)$$

$$\frac{dp^{ch}_{H_2O}}{dt} = \frac{RT}{V_a}\left[\frac{2M_a}{P^{ch}_a}\left(p^{in}_{H_2O} - p^{ch}_{H_2O}\right) - \frac{i}{2F}\right] \quad (31)$$

$$\frac{dp^{ch}_{O_2}}{dt} = \frac{RT}{V_a}\left[\frac{2M_a}{P^{ch}_a}\left(p^{in}_{O_2} - p^{ch}_{O_2}\right) - \frac{i}{2F}\right] \quad (32)$$

The CF voltage for single fuel cell can be expressed mathematically as [57]:

$$V_{CF} = n_{CF} V_{Cell} \quad (33)$$

E. MODEL DEVELOPMENT OF ELECTROLYZER

There are three main technologies that can be adopted for the electrolysis process of proton exchange, such as: Solid Oxide Electrolyzer (SOE), Alkaline Electrolyzer, Membrane Electrolyzer. The temperature operating range of SOE systems is very high such as 550-1100 °C therefore, such a high temperature does not require expensive catalysts and enhances integrating potential and conversion efficiency of the system. Furthermore, the input energy which is required for SOE system can be minimized if excess heat sources for water or steam are reused due to high temperature. The decomposition of water into hydrogen and oxygen is obtained by flow of current through electrolyzer which is shown by the empirical V_{Elec}, I_{Elec} equation written as [58] and [53]:

$$V_{Elec} = U_{rev} + \frac{r_1 + r_1 T}{A_{Elec}} I_{Elec} + k \quad (34)$$

$$k = k_{Elec}\, ln\left[(k_{T_1} + (\frac{k_{T_2}}{T}) + (\frac{k_{T_3}}{T^2}))\frac{I_{Elec}}{A_{Elec}} + 1\right] \quad (35)$$

where, r_1 and r_2 denote ohmic resistances whereas, k_{Elec}, k_{T_1}, k_{T_2}, and k_{T_3} are the factors of the overvoltage of electrolyzer. Moreover, A_{Elec} represents area of the electrode cell.

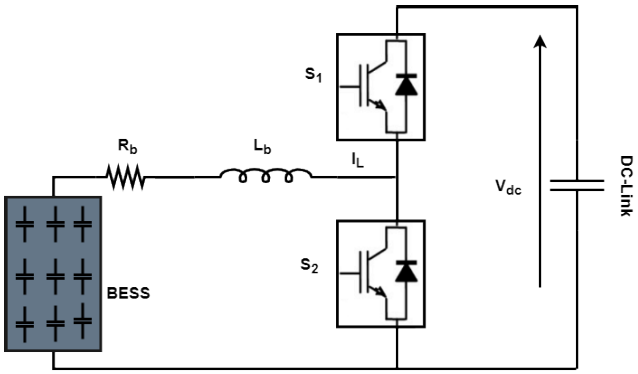

FIGURE 6. Schematic diagram of DC-DC converter associated with BESS.

IV. POWER MANAGEMENT

The main goal of any topology of the management of power is to assure an adequate quality of power according to the form of energy which is stored. All the energy sources that are being proposed were investigated to examine the topology of the management of power. Charging as well as discharging of BESS is dependent upon the power consumption of the hybrid system. Therefore, BESS is interfaced with the DC-link by using a DC-DC converter that serves as a charge controller. This controller allows both negative and positive currents to flow from the BESS to the DC-link and from the DC link to the BESS during its charging mode and its discharging mode. Output voltage of the BESS is uni-polar so, the polarity of the voltage of the battery does not alter. Moreover, converter of DC-DC possesses first quadrant and the second quadrant functionalities [59]. DC-DC converter for BESS is presented in Fig. 6, and the associated equation can be obtained as:

$$L_b \frac{di_L}{dt} = V_{dc}\, m_b - V_b - R_b\, i_L \quad (36)$$

where i_L is the BESS current, V_b is the BESS voltage, m_b is the index of modulation. The battery current reference has been generated by taking the ratio of P_{extra} divided by BESS voltage. An error has been taken between BESS current reference and BESS inductor current and injected into the PI controller to generate the duty cycles.

The procedure to find out the current loop reference current commands for the BESS are:

- P_{extra} is equivalent to the difference among the powers of the PV, GSC rating, Rotor and FC:

$$P_{extra} = P_{PV} - P_{GSC} - P_r + P_{FC} \quad (37)$$

- The amount of extra power is represented by P_{extra} that is injected/absorbed by the BESS. The value of P_{extra} is positive when wind speed and solar radiations are high therefore, BESS is meant to absorb this extra power. However, when there is low solar radiation or low wind speed, this power is negative, it depicts that BESS is meant to inject this negative power to the link of DC.

Fig. 7 demonstrates the strategy of control for the charge controller of BESS. Figs. 8 and 9 shows the DC-DC Boost

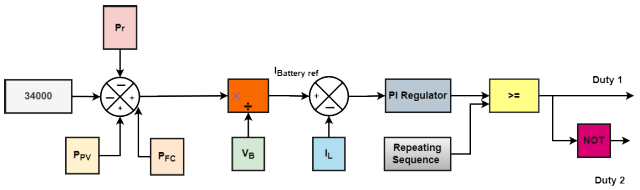

FIGURE 7. Schematic diagram of control associated with BESS.

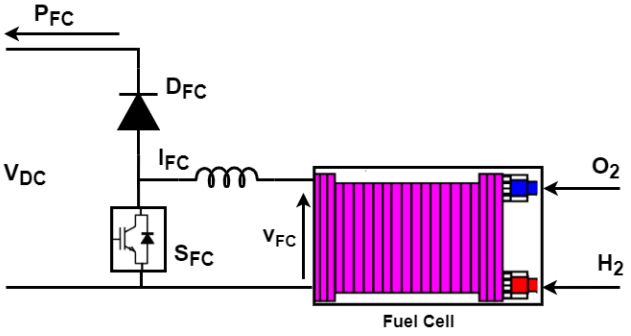

FIGURE 8. Schematic diagram of DC-DC converter controller incorporated with FC.

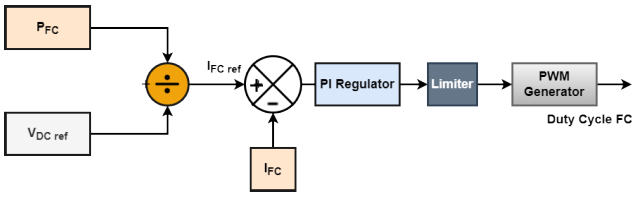

FIGURE 9. Schematic diagram of control associated with FC.

controller associated with FC and duty cycle control angle respectively. Figs. 10 and 11 shows the buck converter and control algorithm for Electrolyzer. The duty cycle for the Electrolyzer is generated by taking the error between V_dc and the power of the Electrolyzer. PI controller is proposed for minimizing the error to achieve the duty cycle for the Electrolyzer by eliminating the steady-state error. The limiter is added to the PI controller for keeping the value of the control duty cycle value between 0 and 1.

In this work, the charging and discharging of BESS are taken with the SoC range of 20% to 80%. Depending upon weather and power requirement, BESS can be considered as a power or sink source. The FC controller and BESS are created in situations where there is an unexpected change in the demand of power, in which BESS gives quick power and the power supply of the BESS ought to be decreased, by increasing the output power of the Fuel Cell. In order to accomplish the link between the BESS and the FC, a DC boost controller combined with a FC is being proposed, expecting a zero-battery current.

Additionally, the FC ought to be replaced by the BESS for such situation where the SoC of the battery is at 20% in order to give power. So, the excessive produced power is being used for the charging of the battery till its cutoff. The

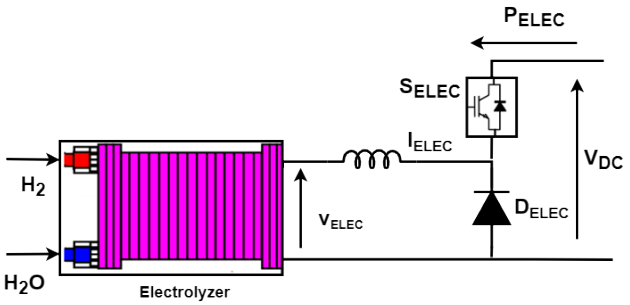

FIGURE 10. Schematic diagram of Electrolyzer with buck converter.

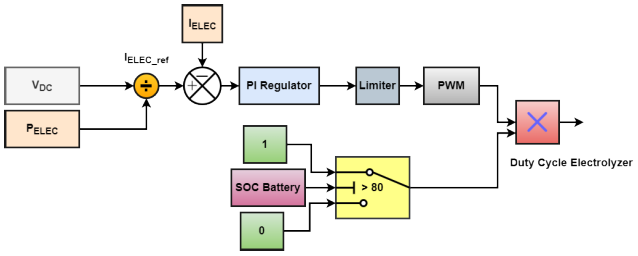

FIGURE 11. Schematic diagram of Electrolyzer control.

remaining power is transmitted to the electrolyzer through a DC converter that is controlled to increase the duty cycle to boost the voltage on the DC grid when the SoC reaches its limit (80%). For appropriate working of the Electrolyzer, when SoC of the battery is greater than 80% and $P_NET > 0$, power flows start to the electrolyzer. In this case, Switch gives the signal to the PI output. The generated FC power can be expressed as:

$$P_{FC} = P_{NET} - P_{BESS} - P_{ELEC} - P_{PV} \tag{38}$$

The control strategies and the proposed management assure that the average power from BESS and the instantaneous power from the FC work as per the SoC of the battery. During charging mode, the Electrolyzer should store extra power when SoC comes to 80% and it begins to produce the hydrogen, which is being reserved in the tank. On the other hand, in the discharging mode of the battery, when the SOC drops to 20%, the FC should indicate lack of power. Additionally, when there is low demand $P_{NET} > 0$ or more wind power, the extra power is utilized for the charging of BESS until it reaches the limit (80%). Then, working of the battery is upheld by the Electrolyzer by retaining the extra power. When there is less power generation from PV and Wind, the BESS provides the power that is required by FC, even in high demand ($P_{NET} < 0$), assuring the assistance progression up to the lower limit of SoC. Therefore, the DC-grid voltage (V_{dc}) control is being assured by the related BESS, FC, Electrolyzer and PV, as per the flowchart given by Fig. 12.

V. SIMULATION AND RESULTS

In this paper, the FC and Electrolyzer have been added to WTG-DFIG, PV and BESS systems connected in a hybrid grid system. The hybrid grid-connected system has been

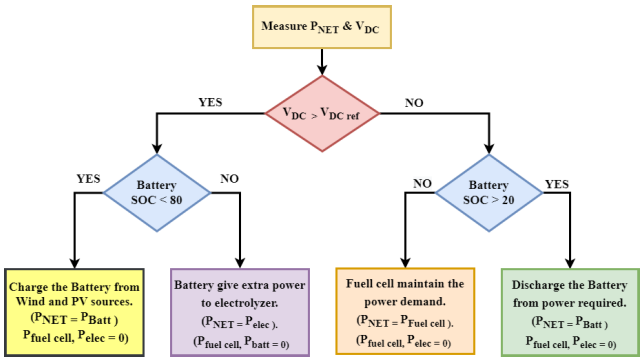

FIGURE 12. Flowchart of power management of all energy sources.

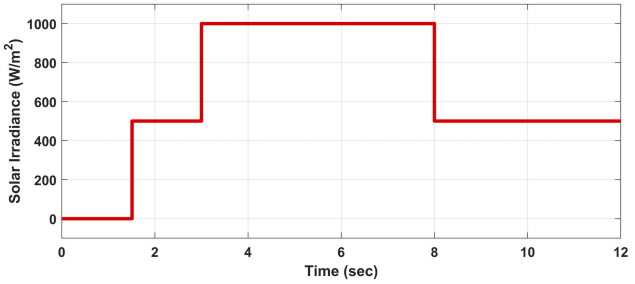

FIGURE 13. Solar Irradiance ($\frac{W}{m^2}$).

implemented and power management for the proposed system is performed in the Simulink environment of MATLAB. The entire system was simulated under different environmental conditions and variable loads. This emphasizes the impacts of this hybrid system on the efficiency and quality of the injected and/or necessary energy.

The capacity of the DFIG is taken as 2 MW along with the solar system that has a capacity more than GSC rating. Generally, GSC and RSC ratings are supposed to be 24% to 31% of the rating of the generator [52]. Thus, GSC and RSC ratings are taken as 340 kVA and 250 kVA, respectively. Contrarily, the PV system rating is taken as 1.1 MW. In order to emphasize the benefits of chosen system, the capacity of the system is considerably taken larger than its GSC rating. A 100-Ah BESS is connected to this system to protect the GSC from overloads. FC of 50 kW and 625 V with an electrolyzer of 35V is added to the system. The DFIG, WT and GSC parameters are given in Table 1.

The proposed system is simulated under various scenarios and the results are provided and analyzed in this section. Solar irradiance is considered to vary across a day as shown in Fig. 13.

The PV system is protected by using diode (D1) and circuit breaker (SP). The circuit breaker is initiated at t = 0. Till t = 2 sec, solar irradiance is 0 W/m^2, then it changes to 500 W/m^2 during t = 2sec to 3 sec, 1000 W/m^2 during 3 to 8 sec and come back to 500 W/m^2 for rest of the time. PV power depends upon the solar irradiance. Fig. 14 shows the PV array type current and power at MPPT. The PV, BESS,

TABLE 1. DFIG, Wind turbine and GSC parameters.

Symbol	Parameter	Values
f	Frequency (Hz)	50
P_s	Rated Stator power (W)	2e6
n	Rated Rotational Speed (rpm)	1500
I_s	Rated Stator current (A)	1760
V_s	Rated Stator voltage (V)	690
T_{em}	Rated Torque (N.m)	12732
p	Pole pair	2
u	Stator/Rotor Turn Ratio	1/3
V_r	Rotor rated voltage (Non-Reached) (V)	2070
s_{max}	Maximum Slip	1/3
C_b	Rated Rotor voltage reference to stator	$(V_r * S_{max}) * u$
R_s	Stator leakage	$2.6e-3$
L_{si}	Leakage Inductance (stator and rotor) (H)	$0.087e-3$
L_m	Magnetization Inductance (H)	$2.5e-3$
R_r	Rotor resistance referred to stator (Ω)	$2.6e-3$
-	Stator Inductance (H)	$L_s = L_m + L_{si}$
-	Rotor Inductance (H)	$L_r = L_m + L_{si}$
V_{dc}	DC link voltage	$1050 - 1150$
J	Inertia	127
f_{sw}	Switching Frequency	$4e3$
N	Gearbox ratio	100
ρ	Air Density	1.225
β	Pitch angle	0
-	C_{pmax}	0.44
C_{bus}	DC bus capacitance	$80e^{-3}$
R_g	Grid side filter resistance	$20e^{-6}$
L_g	Grid side filter inductance	$400e^{-6}$

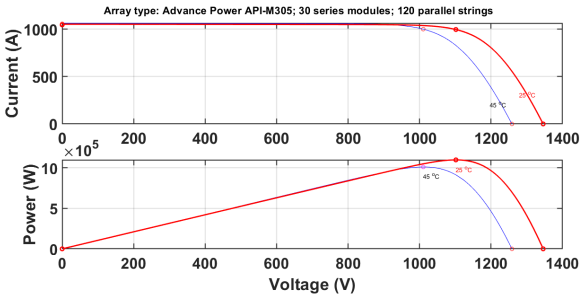

FIGURE 14. Current and Power at MPPT for array type (temperature variation).

FC and Electrolyzer design parameters have been given in Table 2.

PV generation during 3 to 8 sec is maximum and achieved its maximum power of 1.1 MW while operating at MPP. During this internal, PV is supposed to infuse energy into the bus (DC). At this stage, power from the PV and the rotor goes to GSC. This huge power should be utilized well in order to avoid GSC overheating. The output power of PV for the proposed system is presented in Fig. 15. Therefore, BESS continues to start charging and absorb the extra power until

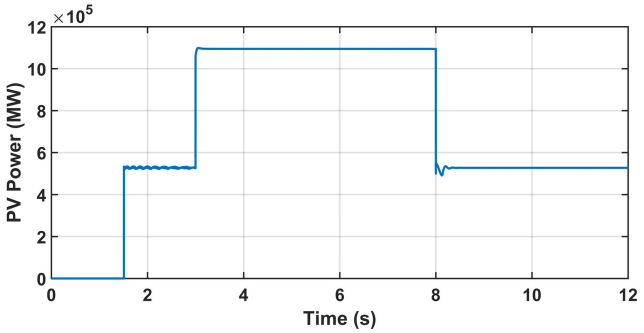

FIGURE 15. PV power (MW).

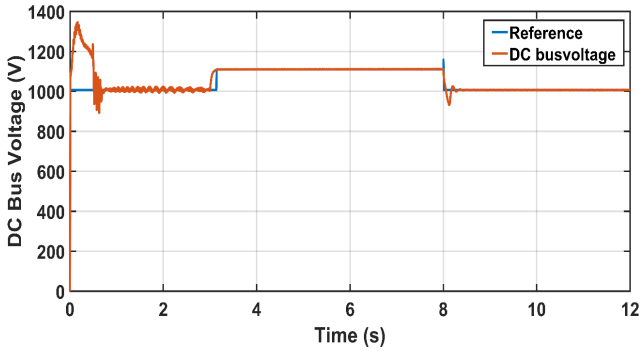

FIGURE 16. DC Bus Voltage (V).

its SOC goes greater than 80%. After 8 sec, solar irradiance drops due to which power generation from the PV goes down, BESS released stored energy to DC link in low solar irradiance condition. DC link waveform has been illustrated in Fig. 16. Before the operation of PV power generation, some initial transients occur but soon DC link voltage maintains at the value of 1000 V due to the BESS power supply. Between 3 to 8 sec, DC link voltage achieves its reference level of 1158 V due to injection of power by PV.

The charging and discharging behavior of BESS when P_{NET} is positive at the DC link, has been demonstrated. Fig. 17 shows the BESS power when the DC link is not getting surplus power from PV. It depicts that BESS is fully discharged between 1 to 2 sec and after 8 sec. Negative power shows the charging behavior of BESS when PV generation track MPP power between 3 to 8 sec. BESS SoC is limited between 20% and 80%. AT SoC $\geq$ 80%, the purpose of BESS at this stage is to discharge the power to the DC link until its SoC comes to 20%. During the initial transient behavior of the system, the BESS is charged. During the second phase, the BESS started discharging till 3 sec to support the power at the DC link and its gets charged when enough power from the PV side ensures the power demand at the DC link.

When BESS is charged at 80% and there is still excess power at the DC link, Electrolyzer starts dissipating power to produce and stored H_2 in the hydrogen tank. When BESS is at 20%, FC gets connected to ensure system stability and service continuity. FC then used the stored H_2 from the hydrogen

TABLE 2. PV, BESS, FC and Electrolyzer design parameters.

Parameter	Values
PV parallel strings	60
Series connected modules per strings	30
Maximum power PV array (W)	213.15
Open circuit voltage V_{oc} (V)	36.3
Short circuit current I_{sc}	7.84
BESS nominal voltage (V)	800
BESS rated capacity (Ah)	100
Initial SoC BESS	50
FC Power (kW)	50
FC Voltage	625
Nominal hydrogen utilization	99.56

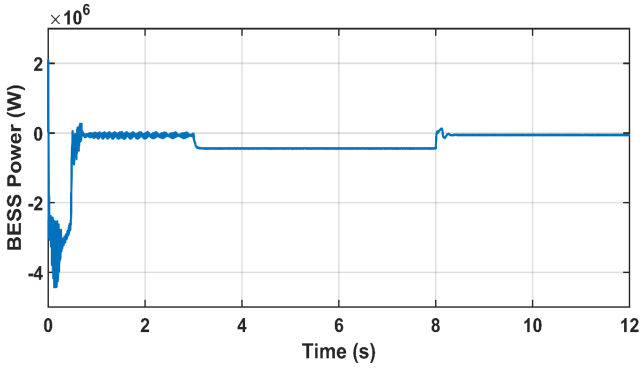

FIGURE 17. BESS discharging power (kW).

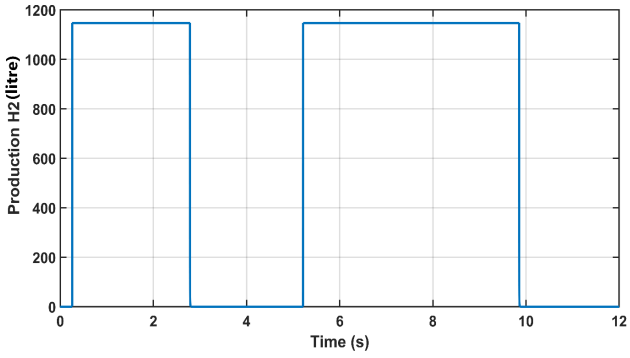

FIGURE 18. H_2 production (litre).

tank to generate power for the supply to the DC link. Figs. 18 and 19 show the H_2 production and storage in hydrogen tank during charging phase of BESS. Fig. 20 illustrated H_2 usage by Fuel Cell in discharging phase of BESS when SoC came down to 20%. Similarly, H_2 production by Electrolyzer and consumption by FC when BESS starts charging are shown in Figs. 21 and 22.

The plots of the rotor powers (Active P_r) and the (Reactive Q_r) are presented in Figs. 23 and 24. In the sub synchronous span, both powers are positive and these powers are being drawn from the RSC while in the super synchronous span, when both powers are negative, it supplies power to

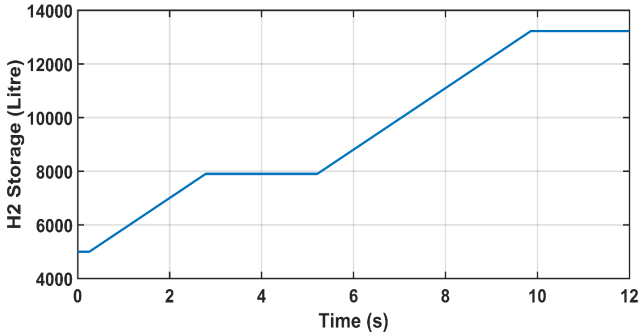

FIGURE 19. H_2 storage (litre).

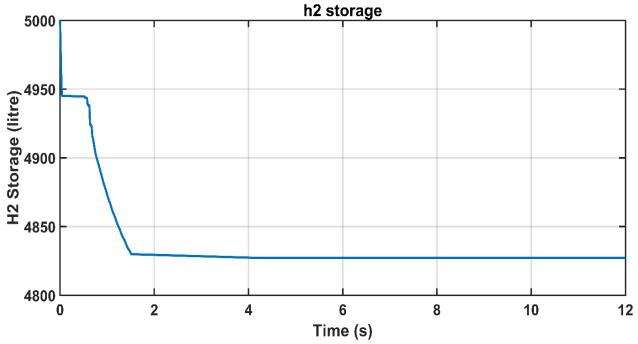

FIGURE 20. H_2 storage (litre) used in discharging case of BESS.

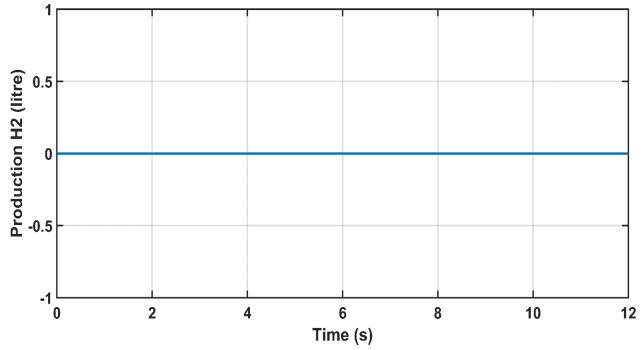

FIGURE 21. H_2 production (litre) in charging state of BESS.

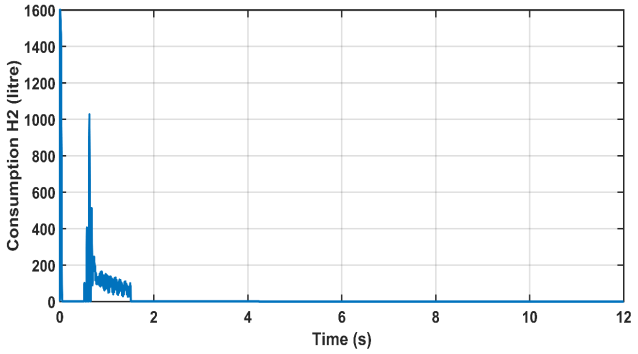

FIGURE 22. H_2 consumption (Charging case).

the DC link. Figs. 25 and 26 illustrate the behavior of stator active and reactive powers respectively. Reactive power is negligible, equals to zero and the active power is positive and delivered to the grid.

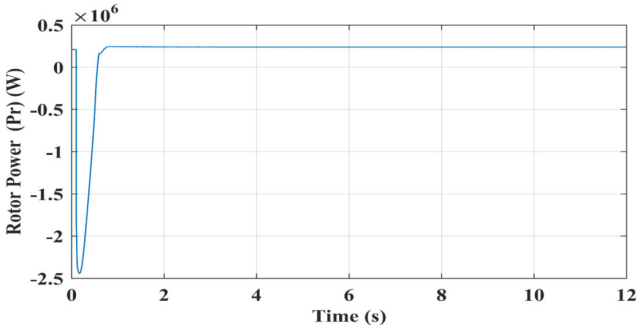

FIGURE 23. Rotor(Pr) power (W).

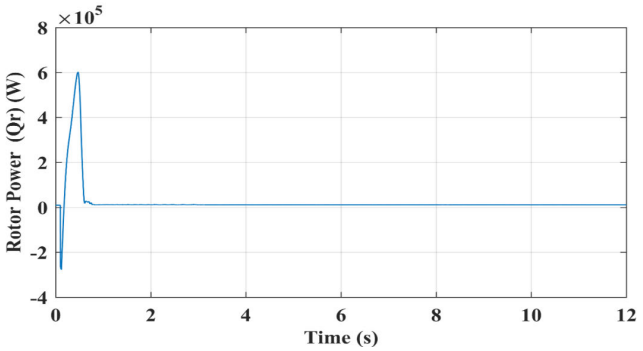

FIGURE 24. Rotor (Qr power (W).

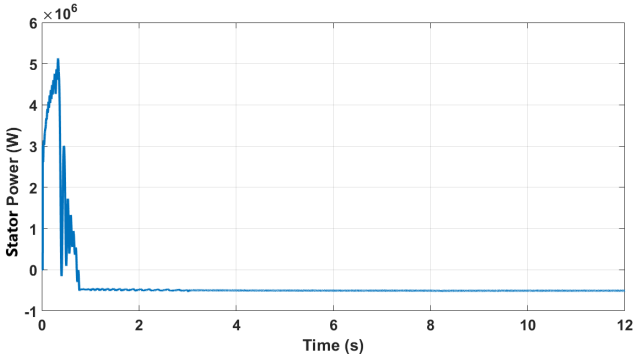

FIGURE 25. Stator (Ps) power (W).

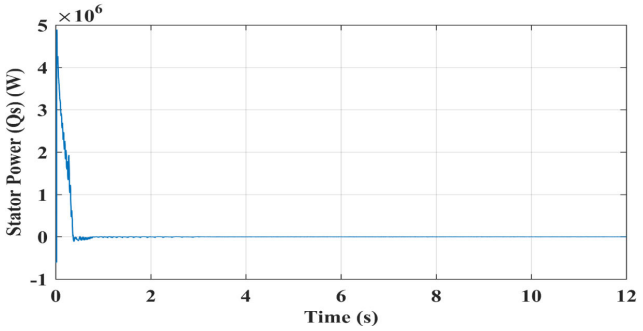

FIGURE 26. Stator (Qs) power (W).

Fig. 27 shows the GSC power waveform. Its value is smaller than its rated value in sub-synchronous mode when PV irradiance or wind velocities are low. However, for proper control of BESS and GSC, its value is kept near to the value which is rated. The performance of this grid voltage is represented in Fig. 28. The main objective of the proposed

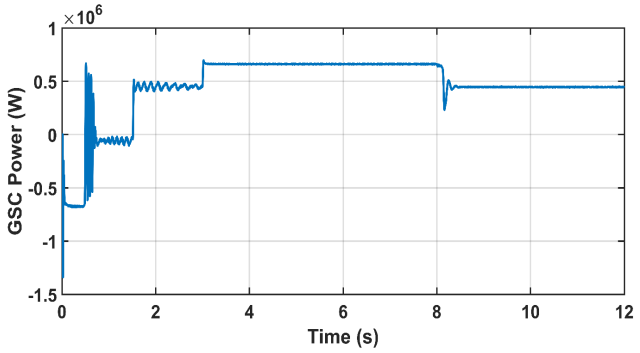

FIGURE 27. P_{GSC} power (W).

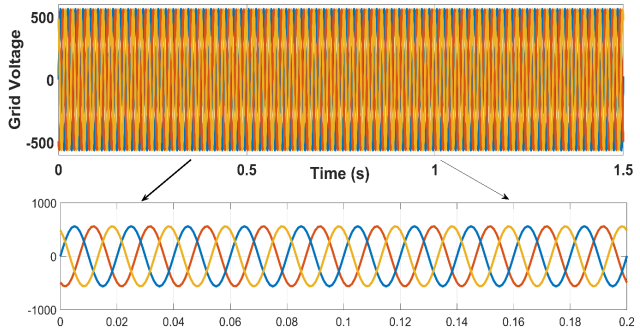

FIGURE 28. Grid Voltage (V).

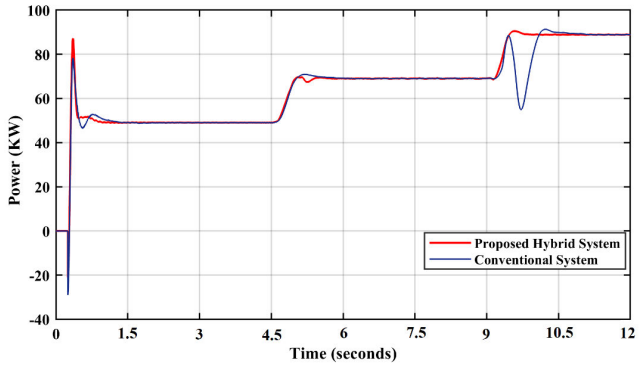

FIGURE 29. Comparative analysis of proposed hybrid and conventional power system.

system is to keep the system and its voltage stable, thus the zoom-in also shows the stable AC grid voltage.

Fig. 29 shows the output power response of the proposed hybrid system and the conventional system. In the proposed design fuel cell and PV contribute to achieving the reference target by meeting the energy demand.

VI. CONCLUSION

In this paper, FC and Electrolyzer as an energy source have been added to the PV-DFIG and BESS hybrid grid connected system with the least number of converter and control loops is proposed. The characteristics of all system components and main configuration of the proposed system are explained. This paper includes the design of controllers for grid-connected hybrid systems with renewable distributed generators (Wind and PV) as a primary source, BESS as a secondary source and FC with Electrolyzer as a tertiary source. The proposed hybrid system presents a cost efficient solution for integrating PV into a hybrid system by eliminating the converter of the PV. The system that is being proposed is controlled by introducing power management for better power sharing between proposed sources. PV power is maximized and injected into the grid through GSC. BESS with coordination of FC and Electrolyzer eliminates the effect of intermittency of power generated from wind and PV. Excess power production by renewable distribution generation is used by Electrolyzer to generate hydrogen. This hydrogen is further used by FC when there is not enough power generation due to unfavorable weather conditions. The power management is presented to fulfill the load profile, avoid BESS overcharging and to minimize the intermittency and fluctuation of Wind and PV sources. This method guarantees a steady power flow and service continuity. Significant improvement has been observed by introducing FC with Electrolyzer to the Wind/PV/BESS-based hybrid grid connected system. Better power management, DC link voltage tracking and MPP of PV power from the GSC side have been observed.

This work can be further improved by introducing nonlinear controllers to better cater nonlinearities presented in Wind, Fuel Cell, Electrolyzer and BESS for the proposed hybrid grid-connected system. Moreover, an Artificial intelligence-based algorithm can be implemented for power management.

REFERENCES

[1] J. M. Carrasco, L. G. Franquelo, J. T. Bialasiewicz, E. Galván, R. C. PortilloGuisado, M. M. Prats, J. I. León, and N. Moreno-Alfonso, "Power-electronic systems for the grid integration of renewable energy sources: A survey," *IEEE Trans. Ind. Electron.*, vol. 53, no. 4, pp. 1002–1016, Jun. 2006.

[2] H. HassanzadehFard, F. Tooryan, E. R. Collins, S. Jin, and B. Ramezani, "Design and optimum energy management of a hybrid renewable energy system based on efficient various hydrogen production," *Int. J. Hydrogen Energy*, vol. 45, no. 55, pp. 30113–30128, Nov. 2020.

[3] M. Xie, M. M. Gulzar, H. Tehreem, M. Y. Javed, and S. T. H. Rizvi, "Automatic voltage regulation of grid connected photovoltaic system using Lyapunov based sliding mode controller: A finite—Time approach," *Int. J. Control, Autom. Syst.*, vol. 18, no. 6, pp. 1550–1560, Jun. 2020.

[4] F. U. Khan, M. M. Gulzar, D. Sibtain, H. M. Usman, and A. Hayat, "Variable step size fractional incremental conductance for MPPT under changing atmospheric conditions," *Int. J. Numer. Model., Electron. Netw., Devices Fields*, vol. 33, no. 6, p. e2765, Nov. 2020.

[5] K. A. Khan and M. Khalid, "Improving the transient response of hybrid energy storage system for voltage stability in DC microgrids using an autonomous control strategy," *IEEE Access*, vol. 9, pp. 10460–10472, 2021.

[6] J. Yao, H. Li, Y. Liao, and Z. Chen, "An improved control strategy of limiting the DC-link voltage fluctuation for a doubly fed induction wind generator," *IEEE Trans. Power Electron.*, vol. 23, no. 3, pp. 1205–1213, May 2008.

[7] B. Benlahbib, N. Bouarroudj, S. Mekhilef, D. Abdeldjalil, T. Abdelkrim, F. Bouchafaa, and A. Lakhdari, "Experimental investigation of power management and control of a PV/wind/fuel cell/battery hybrid energy system microgrid," *Int. J. Hydrogen Energy*, vol. 45, no. 53, pp. 29110–29122, Oct. 2020.

[8] A. Khan, H. Ahmad, S. M. Ahsan, M. M. Gulzar, and S. Murawwat, "Coordinated LVRT support for a PMSG-based wind energy conversion system integrated into a weak AC-grid," *Energies*, vol. 14, no. 20, p. 6588, Oct. 2021.

[9] J. P. Da Costa, H. Pinheiro, T. Degner, and G. Arnold, "Robust controller for DFIGs of grid-connected wind turbines," *IEEE Trans. Ind. Electron.*, vol. 58, no. 9, pp. 4023–4038, Sep. 2011.

[10] C. Liu, F. Blaabjerg, W. Chen, and D. Xu, "Stator current harmonic control with resonant controller for doubly fed induction generator," *IEEE Trans. Power Electron.*, vol. 27, no. 7, pp. 3207–3220, Jul. 2011.

[11] H. Xu, J. Hu, and Y. He, "Operation of wind-turbine-driven DFIG systems under distorted grid voltage conditions: Analysis and experimental validations," *IEEE Trans. Power Electron.*, vol. 27, no. 5, pp. 2354–2366, May 2012.

[12] H. Nian and Y. Song, "Direct power control of doubly fed induction generator under distorted grid voltage," *IEEE Trans. Power Electron.*, vol. 29, no. 2, pp. 894–905, Feb. 2014.

[13] M. M. Gulzar, D. Sibtain, A. F. Murtaza, S. Murawwat, M. Saadi, and A. Jameel, "Adaptive fuzzy based optimized proportional-integral controller to mitigate the frequency oscillation of multi-area photovoltaic thermal system," *Int. Trans. Electr. Energy Syst.*, vol. 31, no. 1, 2021, Art. no. e12643.

[14] Z. Dejia, Z. Zhengming, M. Eltawil, and Y. Liqiang, "Design and control of a three-phase grid-connected photovoltaic system with developed maximum power point tracking," in *Proc. 23rd Annu. IEEE Appl. Power Electron. Conf. Expo.*, Feb. 2008, pp. 973–979.

[15] M. Gulzar, S. Rizvi, M. Javed, D. Sibtain, and R. S. Ud Din, "Mitigating the load frequency fluctuations of interconnected power systems using model predictive controller," *Electronics*, vol. 8, no. 2, p. 156, Feb. 2019.

[16] M. Maaruf, K. Khan, and M. Khalid, "Robust control for optimized islanded and grid-connected operation of solar/wind/battery hybrid energy," *Sustainability*, vol. 14, no. 9, p. 5673, May 2022.

[17] M. Hanan, X. Ai, M. Y. Javed, M. Majid Gulzar, and S. Ahmad, "A two-stage algorithm to harvest maximum power from photovoltaic system," in *Proc. 2nd IEEE Conf. Energy Internet Energy Syst. Integr. (EI2)*, Oct. 2018, pp. 1–6.

[18] H. Ghoddami, M. B. Delghavi, and A. Yazdani, "An integrated wind-photovoltaic-battery system with reduced power-electronic interface and fast control for grid-tied and off-grid applications," *Renew. Energy*, vol. 45, pp. 128–137, Sep. 2012.

[19] R. G. Wandhare and V. Agarwal, "Novel integration of a PV-wind energy system with enhanced efficiency," *IEEE Trans. Power Electron.*, vol. 30, no. 7, pp. 3638–3649, Jul. 2015.

[20] M. Y. Javed, M. M. Gulzar, S. T. H. Rizvi, and A. Arif, "A hybrid technique to harvest maximum power from PV systems under partial shading conditions," in *Proc. Int. Conf. Emerg. Technol. (ICET)*, Oct. 2016, pp. 1–5.

[21] S. Diaf, G. Notton, M. Belhamel, M. Haddadi, and A. Louche, "Design and techno-economical optimization for hybrid PV/wind system under various meteorological conditions," *Appl. Energy*, vol. 85, no. 10, pp. 968–987, Oct. 2008.

[22] B. N. Alhasnawi, B. H. Jasim, Z.-A.-S. A. Rahman, and P. Siano, "A novel robust smart energy management and demand reduction for smart homes based on internet of energy," *Sensors*, vol. 21, no. 14, p. 4756, Jul. 2021.

[23] S. Dorahaki, R. Dashti, and H. R. Shaker, "Optimal energy management in the smart microgrid considering the electrical energy storage system and the demand-side energy efficiency program," *J. Energy Storage*, vol. 28, Apr. 2020, Art. no. 101229.

[24] T. M. Gür, "Review of electrical energy storage technologies, materials and systems: Challenges and prospects for large-scale grid storage," *Energy Environ. Sci.*, vol. 11, no. 10, pp. 2696–2767, 2018.

[25] Y. Alhumaid, K. Khan, F. Alismail, and M. Khalid, "Multi-input nonlinear programming based deterministic optimization framework for evaluating microgrids with optimal renewable-storage energy mix," *Sustainability*, vol. 13, no. 11, p. 5878, May 2021.

[26] M. Khalid, "A review on the selected applications of battery-supercapacitor hybrid energy storage systems for microgrids," *Energies*, vol. 12, no. 23, p. 4559, Nov. 2019.

[27] H. T. Dinh, J. Yun, D. M. Kim, K. Lee, and D. Kim, "A home energy management system with renewable energy and energy storage utilizing main grid and electricity selling," *IEEE Access*, vol. 8, pp. 49436–49450, 2020.

[28] A. Khatamianfar, M. Khalid, A. V. Savkin, and V. G. Agelidis, "Improving wind farm dispatch in the Australian electricity market with battery energy storage using model predictive control," *IEEE Trans. Sustain. Energy*, vol. 4, no. 3, pp. 745–755, Jul. 2013.

[29] D. Sibtain, A. F. Murtaza, N. Ahmed, H. A. Sher, and M. M. Gulzar, "Multi control adaptive fractional order PID control approach for PV/wind connected grid system," *Int. Trans. Electr. Energy Syst.*, vol. 31, no. 4, 2021, Art. no. e12809.

[30] C. Ghenai, M. Bettayeb, B. Brdjanin, and A. K. Hamid, "Hybrid solar PV/PEM fuel cell/diesel generator power system for cruise ship: A case study in Stockholm, Sweden," *Case Stud. Thermal Eng.*, vol. 14, Sep. 2019, Art. no. 100497.

[31] M. Çolak and İ. Kaya, "Multi-criteria evaluation of energy storage technologies based on hesitant fuzzy information: A case study for Turkey," *J. Energy Storage*, vol. 28, Apr. 2020, Art. no. 101211.

[32] L. Kong, J. Yu, and G. Cai, "Modeling, control and simulation of a photovoltaic/hydrogen/supercapacitor hybrid power generation system for grid-connected applications," *Int. J. Hydrogen Energy*, vol. 44, no. 46, pp. 25129–25144, Sep. 2019.

[33] R. Amirante, E. Cassone, E. Distaso, and P. Tamburrano, "Overview on recent developments in energy storage: Mechanical, electrochemical and hydrogen technologies," *Energy Convers. Manage.*, vol. 132, pp. 372–387, Jan. 2017.

[34] U. Akram and M. Khalid, "A coordinated frequency regulation framework based on hybrid battery-ultracapacitor energy storage technologies," *IEEE Access*, vol. 6, pp. 7310–7320, 2017.

[35] Z. Wang, Y. Jia, C. Cai, Y. Chen, N. Li, M. Yang, and Q. Li, "Study on the optimal configuration of a wind-solar-battery-fuel cell system based on a regional power supply," *IEEE Access*, vol. 9, pp. 47056–47068, 2021.

[36] K. A. Khan and M. Khalid, "Hybrid energy storage system for voltage stability in a DC microgrid using a modified control strategy," in *Proc. IEEE Innov. Smart Grid Technol. Asia (ISGT Asia)*, May 2019, pp. 2760–2765.

[37] T. Ma, H. Yang, and L. Lu, "Development of hybrid battery–supercapacitor energy storage for remote area renewable energy systems," *Appl. Energy*, vol. 153, pp. 56–62, Sep. 2015.

[38] M. M. Gulzar, M. Iqbal, S. Shahzad, H. A. Muqeet, M. Shahzad, and M. M. Hussain, "Load frequency control (LFC) strategies in renewable energy-based hybrid power systems: A review," *Energies*, vol. 15, no. 10, p. 3488, May 2022.

[39] L. Zhang, X. Hu, Z. Wang, F. Sun, and D. G. Dorrell, "A review of supercapacitor modeling, estimation, and applications: A control/management perspective," *Renew. Sustain. Energy Rev.*, vol. 81, no. 2, pp. 1868–1878, 2018.

[40] F. Nejabatkhah, S. Danyali, S. H. Hosseini, M. Sabahi, and S. M. Niapour, "Modeling and control of a new three-input DC–DC boost converter for hybrid PV/FC/battery power system," *IEEE Trans. Power Electron.*, vol. 27, no. 5, pp. 2309–2324, May 2012.

[41] Y.-M. Chen, C.-S. Cheng, and H.-C. Wu, "Grid-connected hybrid PV/wind power generation system with improved DC bus voltage regulation strategy," in *Proc. 21st Annu. IEEE Appl. Power Electron. Conf. Expo.*, Mar. 2006, p. 7.

[42] X. Li, D. Hui, and X. Lai, "Battery energy storage station (BESS)-based smoothing control of photovoltaic (PV) and wind power generation fluctuations," *IEEE Trans. Sustain. Energy*, vol. 4, no. 2, pp. 464–473, Apr. 2013.

[43] S. S. Martin, A. Chebak, A. El Ouafi, and M. Mabrouki, "Modeling and simulation of hybrid power system integrating wind, solar, biodiesel energies and storage battery," in *Proc. Int. Renew. Sustain. Energy Conf. (IRSEC)*, Nov. 2016, pp. 457–463.

[44] R. Sebastián, "Battery energy storage for increasing stability and reliability of an isolated wind diesel power system," *IET Renew. Power Gener.*, vol. 11, no. 2, pp. 296–303, Feb. 2017.

[45] B. P. Hayes, A. Wilson, R. Webster, and S. Z. Djokic, "Comparison of two energy storage options for optimum balancing of wind farm power outputs," *IET Gener., Transmiss. Distrib.*, vol. 10, no. 3, pp. 832–839, 2016.

[46] L. Qu and W. Qiao, "Constant power control of DFIG wind turbines with supercapacitor energy storage," *IEEE Trans. Ind. Appl.*, vol. 47, no. 1, pp. 359–367, Jan. 2011.

[47] G. Lei, H. Song, and D. Rodriguez, "Power generation cost minimization of the grid-connected hybrid renewable energy system through optimal sizing using the modified seagull optimization technique," *Energy Rep.*, vol. 6, pp. 3365–3376, Nov. 2020.

[48] M. B. Camara, B. Dakyo, and H. Gualous, "Polynomial control method of DC/DC converters for DC-bus voltage and currents management—Battery and supercapacitors," *IEEE Trans. Power Electron.*, vol. 27, no. 3, pp. 1455–1467, Mar. 2012.
[49] S. Adhikari and F. Li, "Coordinated V-f and P-Q control of solar photovoltaic generators with MPPT and battery storage in microgrids," *IEEE Trans. Smart Grid*, vol. 5, no. 3, pp. 1270–1281, May 2014.
[50] S. Najafi-Shad, S. M. Barakati, and A. Yazdani, "An effective hybrid wind-photovoltaic system including battery energy storage with reducing control loops and omitting PV converter," *J. Energy Storage*, vol. 27, Feb. 2020, Art. no. 101088.
[51] M. G. Villalva, J. R. Gazoli, and E. R. Filho, "Comprehensive approach to modeling and simulation of photovoltaic arrays," *IEEE Trans. Power Electron.*, vol. 24, no. 5, pp. 1198–1208, May 2009.
[52] G. Abad, J. Lopez, M. Rodriguez, L. Marroyo, and G. Iwanski, *Doubly Fed Induction Machine: Modeling and Control for Wind Energy Generation*. Hoboken, NJ, USA: Wiley, 2011.
[53] Y. Xu and X. Shen, "Optimal control based energy management of multiple energy storage systems in a microgrid," *IEEE Access*, vol. 6, pp. 32925–32934, 2018.
[54] M. Aly, E. M. Ahmed, H. Rezk, and E. A. Mohamed, "Marine predators algorithm optimized reduced sensor fuzzy-logic based maximum power point tracking of fuel cell-battery standalone applications," *IEEE Access*, vol. 9, pp. 27987–28000, 2021.
[55] M. S. Guney and Y. Tepe, "Classification and assessment of energy storage systems," *Renew. Sustain. Energy Rev.*, vol. 75, pp. 1187–1197, Aug. 2017.
[56] S. Buchaniec, A. Sciazko, M. Mozdzierz, and G. Brus, "A novel approach to the optimization of a solid oxide fuel cell anode using evolutionary algorithms," *IEEE Access*, vol. 7, pp. 34361–34372, 2019.
[57] N. Benyahia, H. Denoun, M. Zaouia, T. Rekioua, and N. Benamrouche, "Power system simulation of fuel cell and supercapacitor based electric vehicle using an interleaving technique," *Int. J. Hydrogen Energy*, vol. 40, no. 45, pp. 15806–15814, Dec. 2015.
[58] M. Ceraolo, G. Lutzemberger, and D. Poli, "State-of-charge evaluation of supercapacitors," *J. Energy Storage*, vol. 11, pp. 211–218, Jun. 2017.
[59] A. M. Trzynadlowski, *Introduction to Modern Power Electronics*. Hoboken, NJ, USA: Wiley, 2015.

MUHAMMAD MAJID GULZAR received the M.S. degree in electrical engineering (control science and engineering) from the University of Engineering and Technology (UET), Lahore, Pakistan, in 2012, the Ph.D. degree in electrical engineering (control science and engineering) from the University of Science and Technology of China (USTC), in 2016, and the Postdoctorate Certification from the Nanjing University of Aeronautics and Astronautics, Nanjing, China, in 2019. He is currently an Assistant Professor with the Control and Instrumentation Engineering (CIE) Department, King Fahd University of Petroleum and Minerals (KFUPM), Saudi Arabia. Before joining KFUPM, he was a Lecturer/Assistant Professor/Associate Professor with the University of Central Punjab, Pakistan, from 2008 to 2022. His research interests include operation and control of renewable energy systems, optimization techniques and applications, multi-agent networks, analysis and design of linear/nonlinear systems, and economic energy dispatch. He has advised several projects in these areas and has a number of publications in international leading journals and conferences. He is a member of the Center for Renewable Energy and Power Systems, KFUPM, the Pakistan Engineering Council (PEC), and IEEEP (P).

AYESHA IQBAL received the bachelor's and master's degrees in electrical engineering from the University of Central Punjab (UCP), Lahore, Pakistan. She is affiliated with the Department of Electrical Engineering at UCP. She has also been working with the Solar Company, Pakistan. Her research interests include renewable energy systems, control systems, and solar PV.

DAUD SIBTAIN received the B.Sc. and M.Sc. degrees from the University of Central Punjab (UCP), Lahore, Pakistan, where he is currently pursuing the Ph.D. degree. He is also with the Energy Center of Excellence (ECoE). He is the author/coauthor of more than 15 research articles. His research interests include the design of solar PV converters, IV curve tracing, renewable-based interconnected gird-control designs, hybrid electric vehicle (HEV) control, and load frequency control (LFC) problems for multi-area power systems.

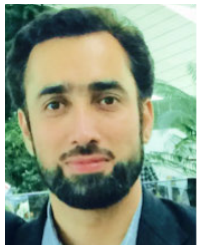

MUHAMMAD KHALID (Senior Member, IEEE) received the Ph.D. degree in electrical engineering from the School of Electrical Engineering Telecommunications (EET), University of New South Wales (UNSW), Sydney, Australia, in 2011. He was a Postdoctoral Research Fellow for three years and then he continued as a Senior Research Associate with the School of EET, Australian Energy Research Institute, UNSW, for another two years. He is currently an Associate Professor with the Electrical Engineering Department, King Fahd University of Petroleum and Minerals (KFUPM), Dhahran, Saudi Arabia. He has been a Researcher with the K. A. CARE Energy Research Innovation Center, Dhahran. He has authored/coauthored several journal and conference papers in the field of control and optimization for renewable power systems. He has been a reviewer of numerous international journals and conferences. His current research interests include the optimization and control of battery energy storage systems for large-scale grid-connected renewable power plants (particularly wind and solar), distributed power generation and dispatch, hybrid energy storage, EVs, and smart grids. He was a recipient of a highly competitive postdoctoral writing fellowship from UNSW, in 2010. Most recently, he has received a prestigious K. A. CARE Fellowship. He is a member of the Center for Renewable Energy and Power Systems and SDAIA–KFUPM Joint Research Center for Artificial Intelligence, Dhahran.